





Harnessing Wavefront Curvature and Spatial Correlation in Noncoherent MIMO Communications

Aniol Martí , *Graduate Student Member, IEEE*, Luca Sanguinetti , *Fellow, IEEE*,
Meritxell Lamarca , *Member, IEEE*, and Jaume Riba , *Senior Member, IEEE*

Abstract—Noncoherent communication systems have regained interest due to the growing demand for high-mobility and low-latency applications. Most existing studies using large antenna arrays rely on the far-field approximation, which assumes locally plane wavefronts. This assumption becomes inaccurate at higher frequencies and shorter ranges, where wavefront curvature plays a significant role and antenna arrays may operate in the radiative near field. In this letter, we adopt a model for the channel spatial correlation matrix that remains valid in both near and far field scenarios. Using this model, we demonstrate that noncoherent systems can leverage the benefits of wavefront spherical curvature, even beyond the Fraunhofer distance, revealing that the classical far-field approximation may significantly underestimate system performance. Moreover, we show that large antenna arrays enable the multiplexing of various users and facilitate near-optimal noncoherent detection with low computational complexity.

Index Terms—Near field, massive MIMO, multiuser detection, Fraunhofer distance, mmWave/THz communication.

I. INTRODUCTION

LARGE arrays have become a fundamental piece of current and next generation communication systems. Compared to their traditional multiple-input multiple-output (MIMO) counterpart, large arrays exhibit several benefits such as the reduction of small-scale fading and noise, a phenomenon known in literature as channel hardening [1, Sec. 1.3]. In order to fully exploit channel hardening, the receiver typically needs to obtain instantaneous channel state information (CSI) through a training sequence and use it for coherent detection of the transmitted data. However, in high-mobility environments and systems with a large number of users, the training overhead can result in significant performance degradation [2], [3]. A promising alternative is a paradigm shift to noncoherent communications, in which neither transmitter nor receiver have instantaneous CSI but only statistical.

This work was supported by project MAYTE (PID2022-136512OB-C21) by MICIU/AEI/10.13039/501100011033 and ERDF/EU, grant 2021 SGR 01033 by Departament de Recerca i Universitats de la Generalitat de Catalunya and grant 2023 FI “Joan Oró” 00050 by Departament de Recerca i Universitats de la Generalitat de Catalunya and the ESF+. L. Sanguinetti was supported in part by the Italian Ministry of Education and Research (MUR) in the framework of the FoReLab Project (Department of Excellence) and in part by the European Union under the Italian National Recovery and Resilience Plan (NRRP) of NextGenerationEU, partnership on “Telecommunications of the Future” (PE00000001 – Program “RESTART”, Structural Project 6GWINET, Cascade Call SPARKS).

A. Martí, M. Lamarca and J. Riba are with the Departament de Teoria del Senyal i Comunicacions, Universitat Politècnica de Catalunya (UPC), 08034 Barcelona (e-mail: aniol.marti@upc.edu, meritxell.lamarca@upc.edu, jaume.riba@upc.edu).

L. Sanguinetti is with the Dipartimento di Ingegneria dell’Informazione, University of Pisa, 56122 Pisa, Italy (e-mail: luca.sanguinetti@unipi.it).

Large arrays are typically deployed in high frequency systems, as it allows to place more antennas in less space. However, this combination breaks a common assumption of communications: the wavefront at the receiver is planar [4]. The electromagnetic field between a transmitting and a receiving antenna has been usually divided in three regions: the reactive near field, the radiative near field¹ and the far field [5, Sec. 2.2.4]. The reactive and radiative near field are separated by the Fresnel distance, $d_r = 0.62\sqrt{D^3/\lambda}$, whereas the near and far field are divided by the Fraunhofer distance, $d_f = 2D^2/\lambda$, with D the aperture and λ the wavelength.

The origin of the far-field approximation is that at the Fraunhofer distance the total phase error at the antenna is $\pi/8$, and from an antenna theory perspective angles smaller than this can be neglected [5, Sec. 4.4.1]. But, what if the spherical wavefront is assumed beyond the Fraunhofer distance? It is known that near-field communication has some advantages compared to far-field, such as additional degrees of freedom (DoF) [6]. Therefore, is it possible to benefit from the wave curvature beyond the Fraunhofer distance? Indeed, in [4] it was shown that the classical far-field approximation underestimates the achievable spectral efficiency in coherent multiuser MIMO. In this paper, we aim to show that noncoherent systems can also benefit from the spherical curvature beyond the Fraunhofer distance. In addition, we also illustrate that multiuser noncoherent communications can leverage large arrays to multiplex different users and perform near-optimal detection with lower complexity, suggesting that single-user constellations [7] can be employed in the multiuser scenario with negligible penalty if the number of antennas is sufficiently large [8].

II. SYSTEM AND SIGNAL MODEL

We consider a MIMO system with K active single-antenna user equipments (UEs) operating in non-line-of-sight (NLoS) propagation conditions. The base station (BS) is equipped with a uniform planar array (UPA) located in the yz plane, and consisting of N independent radio frequency (RF) chains, arranged into N_V rows, each with N_H antennas: $N = N_H N_V$, as depicted in Fig. 1. The inter-element spacing across horizontal and vertical directions is Δ . The location in Cartesian coordinates of the n -th antenna, with $1 \leq n \leq N$, with respect to the origin is $\mathbf{u}_n = (0, i_n \Delta, j_n \Delta)^T$, where $i_n = \text{mod}(n-1, N_H)$ and $j_n = \lfloor \frac{n-1}{N_H} \rfloor$ are the horizontal and vertical indices of element n . We call $\mathbf{h}_k \in \mathbb{C}^N$ the channel response between the k -th UE and the BS [9].

¹Throughout this paper we only consider the radiative near field and refer to it just as *near field*.

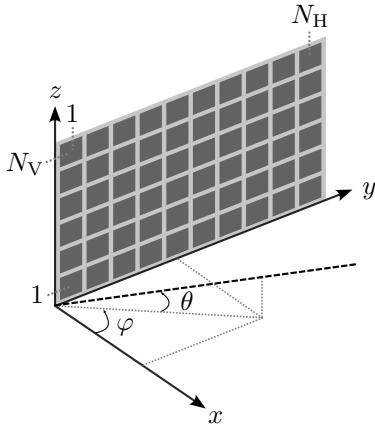


Fig. 1. Geometry of a BS equipped with a $N_H \times N_V$ UPA in the yz plane.

A. Channel Model

Under NLoS conditions, the BS receives a superposition of L multipath components [1, Sec. 1.3]. With scattering localized around each UE and the elevated BS experiencing no near-field scattering, each component produces a wave arriving at the array from a specific direction. When L is sufficiently large, the channel vector follows a complex Gaussian distribution, $\mathbf{h}_k \sim \mathcal{CN}(\mathbf{0}_N, \mathbf{R}_{\mathbf{h}_k})$, with covariance matrix

$$\mathbf{R}_{\mathbf{h}_k} = \mathbb{E}[\mathbf{h}_k \mathbf{h}_k^H] = \sum_{i=1}^L \beta_{ki} \mathbf{a}_{ki} \mathbf{a}_{ki}^H. \quad (1)$$

Here, β_{ki} represents the path gain associated with the i -th scatterer and

$$\mathbf{a}_{ki} = \left(e^{-j\frac{2\pi}{\lambda} \|\mathbf{s}_{ki} - \mathbf{u}_0\|}, \dots, e^{-j\frac{2\pi}{\lambda} \|\mathbf{s}_{ki} - \mathbf{u}_{N-1}\|} \right)^T \quad (2)$$

is the array response vector for the wave arriving from the scatterer located, in spherical coordinates, at $\mathbf{s}_{ki} = (r_{ki}, \theta_{ki}, \varphi_{ki})^T$.

Unlike the classical model, which assumes locally planar wavefronts and only applies in the far field, the above model is valid in the so-called radiative near field of the array [10]. If the k -th UE is in the far field of the array, then \mathbf{h}_k can be approximated as $\mathbf{h}_k^{\text{FF}} \sim \mathcal{CN}(\mathbf{0}_N, \mathbf{R}_{\mathbf{h}_k}^{\text{FF}})$, with $\mathbf{R}_{\mathbf{h}_k}^{\text{FF}}$ given by:

$$\mathbf{R}_{\mathbf{h}_k}^{\text{FF}} = \sum_{i=1}^L \beta_{ki} \mathbf{a}_{ki}^{\text{FF}} (\mathbf{a}_{ki}^{\text{FF}})^H, \quad (3)$$

where the n -th entry of $\mathbf{a}_{ki}^{\text{FF}}$ can be computed as [9]:

$$[\mathbf{a}_{ki}^{\text{FF}}]_n = e^{j\frac{2\pi}{\lambda} \Delta(i_n \cos \theta_{ki} \sin \varphi_{ki} + j_n \sin \theta_{ki})}. \quad (4)$$

B. Signal Model

Consider the uplink of a one-shot² communication system where the transmitted symbols are drawn from an equiprobable M -ary pulse-amplitude modulation (PAM) $\mathcal{X} = \{x_1, \dots, x_M\}$ with $x_1 = 0$ and $\mathbb{E}[|x|^2] = 1$. The complex baseband signal $\mathbf{y} \in \mathbb{C}^N$ received at the BS is:

$$\mathbf{y} = \sum_{k=1}^K \mathbf{h}_k \sqrt{p_k} x_k + \mathbf{z}, \quad (5)$$

²The channel is constant for a single use and information is decoded symbol-by-symbol.

where $\mathbf{z} \sim \mathcal{CN}(\mathbf{0}_N, \mathbf{R}_{\mathbf{z}})$ is additive Gaussian noise, x_k is the PAM symbol transmitted by the k -th UE and p_k is a power control factor such that at the BS all signals have the same signal-to-interference-plus-noise ratio (SINR),

$$\text{SINR} = \frac{p_k \text{tr}(\mathbf{R}_{\mathbf{h}_k})}{\text{tr}(\mathbf{R}_{\mathbf{z}}) + \sum_{j \neq k} p_j \text{tr}(\mathbf{R}_{\mathbf{h}_j})}. \quad (6)$$

As with any noncoherent communication system, the BS is unaware of the realizations of $\{\mathbf{h}_k\}_{k=1}^K$. On the other hand, it may rely on their statistical properties.

The symbol error probability (SER) is:

$$P_e = \frac{1}{MK} \sum_{\mathbf{x} \in \mathcal{X} \times \dots \times \mathcal{X}} \Pr[\hat{\mathbf{x}}(\mathbf{y}) \neq \mathbf{x} | \mathbf{x} = \mathbf{x}], \quad (7)$$

which is minimized by the maximum likelihood (ML) detector [11, Sec. 4.1-1]. This yields

$$\hat{\mathbf{x}}_{\text{ML}} = \arg \min_{\mathbf{x} \in \mathcal{X} \times \dots \times \mathcal{X}} \mathbf{y}^H \mathbf{R}_{\mathbf{y}|\mathbf{x}}^{-1} \mathbf{y} + \log |\mathbf{R}_{\mathbf{y}|\mathbf{x}}|, \quad (8)$$

where

$$\mathbf{R}_{\mathbf{y}|\mathbf{x}} = (\mathbf{x}^T \otimes \mathbf{I}_N) \mathbf{R}_{\text{vec}(\mathbf{H}\mathbf{P})} (\mathbf{x}^* \otimes \mathbf{I}_N) + \mathbf{R}_{\mathbf{z}}, \quad (9)$$

with $\mathbf{x} = (x_1, \dots, x_K)^T$, $\mathbf{H} \in \mathbb{C}^{N \times K} = (\mathbf{h}_1, \dots, \mathbf{h}_K)$ and $\mathbf{P} = \text{diag}(p_1, \dots, p_K)$ the diagonal power control matrix. The column-wise vectorization is denoted by $\text{vec}(\cdot)$ and \otimes is the Kronecker product.

The main drawback of (8) is its complexity, which increases exponentially with K , restricting its practical application to systems with a small number of UEs [11, Sec. 16.3–2]. A suboptimal receiver is the single-user detector that ignores the presence of other users. For the k -th UE, it takes the form:

$$\hat{x}_k = \arg \min_{x \in \mathcal{X}} \mathbf{y}^H \mathbf{R}_{\mathbf{y}|x,k}^{-1} \mathbf{y} + \log |\mathbf{R}_{\mathbf{y}|x,k}|, \quad (10)$$

where

$$\mathbf{R}_{\mathbf{y}|x,k} = |x|^2 p_k \mathbf{R}_{\mathbf{h}_k} + \mathbf{R}_{\mathbf{z}}. \quad (11)$$

In general, the performance gap between (8) and (10) is large. This is not, however, the case for systems with a large number of antennas (compared to the number of users) where the single-user detector achieves near-optimal performance with linear complexity, as we shall demonstrate in the sequel.

In most works on noncoherent communications (see [8] and references therein) uncorrelated Rayleigh fading is assumed, *i.e.* $\mathbf{R}_{\mathbf{h}_k} = \mathbf{I}_N$. However, this model can only be observed in practice if a half-wavelength-spaced uniform linear array in rich scattering is used [12]. On the other hand, the model (1) used in this letter accounts for spatial correlation and is valid not only in the far field but also in the near field. We assume to have perfect knowledge of $\mathbf{R}_{\mathbf{h}_k}$. In line with the MIMO literature at high frequencies, this knowledge can be acquired by means of a model-based acquisition method, which instead of estimating $\mathbf{R}_{\mathbf{h}_k}$ directly, estimates its parameters and constructs the correlation matrix from them. In doing so, it plays a key role the model employed for its computation. In particular, using the far-field model would yield the following

mismatched correlation matrix, even if the parameters are perfectly estimated [4]:

$$\mathbf{R}_{\mathbf{y}|x,k}^{\text{FF}} = |x|^2 p_k \mathbf{R}_{\mathbf{h}_k}^{\text{FF}} + \mathbf{R}_{\mathbf{z}}. \quad (12)$$

The aim of this letter is to quantify the impact of such inaccurate modeling and to provide evidence that a receiver employing (12) instead of (11), even beyond the Fraunhofer distance, significantly underestimates the achievable SER.

C. Single-User Asymptotic Regime

Independently of the receiver considered, a necessary condition for an arbitrarily low P_e in a noncoherent system [13] is to have a *uniquely identifiable constellation*, which in the single-user scenario³ is defined by:

$$|x_a|^2 \neq |x_b|^2 \iff x_a \neq x_b, \quad \forall x_a, x_b \in \mathcal{X}.$$

Under this hypothesis, the error probability exhibits the following properties:

$$\lim_{N \rightarrow \infty} P_e = 0 \iff \lim_{N \rightarrow \infty} \text{rank}(\mathbf{R}_{\mathbf{h}}) = \infty, \quad (13)$$

$$\lim_{p \rightarrow \infty} P_e = 0 \iff M = 2. \quad (14)$$

Although employing large arrays enables lower-complexity detection, the channel rank is still determined by the number of scatterers: $\text{rank}(\mathbf{R}_{\mathbf{h}}) = L$, and it does not increase with N . Therefore, (13) is not fulfilled and the system must exhibit an error floor. Regarding (14), the interpretation is that, for a PAM of order $M = 2$, the zero symbol and the non-zero symbol span different subspaces and can be detected with arbitrarily low error probability. On the other hand, for $M > 2$ all the non-zero symbols share the same subspace and the only vanishing pairwise error probabilities are those between $x_1 = 0$ and any other symbol [14].

III. CHANNEL STATISTICS DISCUSSION

The performance of energy-based noncoherent systems strongly depends on the channel correlation matrix. For this reason, in this section we analyze the main properties of the near-field and far-field models (1) and (3). In doing so, we assume that scattering is local to each UE, with the k -th UE located at $\mathbf{r}_k = (r_k, \theta_k, \varphi_k)^T$, and is uniformly sampled from a sphere centered at the user. We assume that the radius of the sphere is $r_s = 3$ m and the number of scatterers is $L = 10$, unless stated otherwise.

Antennas at the BS are arranged as a UPA with, except where noted, $N = 16 \times 16$ and $\Delta = \lambda$. The system operates at $f = 30$ GHz such that the Fresnel and Fraunhofer distances are $d_r = 0.67$ m and $d_F = 10$ m.

³Note that if the condition is necessary for a single user it must also be necessary in the multiuser scenario.

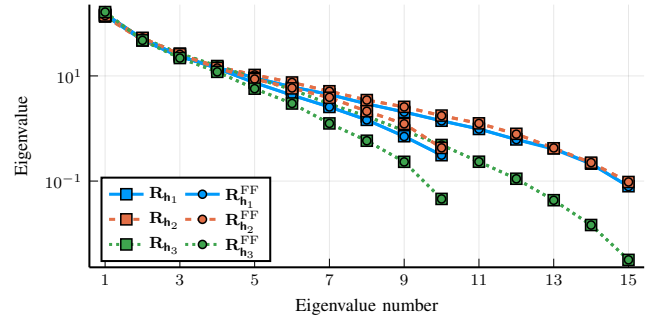


Fig. 2. Non-zero eigenvalues of each UE's near-field and far-field channel correlation matrices for $L = 10$ and $L = 15$.

A. Spatial Correlation Spectrum

We consider two UEs in the near field: $\mathbf{r}_1 = (5, -30^\circ, -10^\circ)$ and $\mathbf{r}_2 = (5, -20^\circ, 0^\circ)$, and a UE in the far field, $\mathbf{r}_3 = (25, -10^\circ, 10^\circ)$. Fig. 2 reports the eigenvalues of $\mathbf{R}_{\mathbf{h}_1}$, $\mathbf{R}_{\mathbf{h}_2}$ and $\mathbf{R}_{\mathbf{h}_3}$, as obtained with (1), and those of their respective far-field matrices, obtained through (3). For all UEs, the eigenvalues of the near-field correlation matrix (rectangular markers) coincide with those of the far-field matrix (circular markers). This shows that both models exhibit the same correlation spectrum. Similar results have been previously observed in [9] and [10].

Regarding the eigenvalues of different users, we should recall that (1) and (3) only depend on the position of the scatterers, but not the user. Thus, if two users are in the same scattering cluster the eigenvalues of their channel correlation matrices coincide, even if scatterers realizations differ. Indeed, for $r_s = 3$ m and two users located at \mathbf{r}_1 and \mathbf{r}_2 , their scatterers overlap and the correlation matrices spectra are very close (see the dashed orange and solid blue lines in Fig. 2).

B. Distance Between Column Spaces

The results in Fig. 2 evidence that the near-field and far-field correlation matrices from (1) and (3) exhibit identical spectra, even at short communication distances. Therefore, the primary difference between the two models must lie in their eigenvectors, *i.e.* $\mathbf{R}_{\mathbf{h}_k}$ and $\mathbf{R}_{\mathbf{h}_k}^{\text{FF}}$ span different subspaces. However, as discussed in Sec. II-C, a noncoherent system such as the one here considered spans only two subspaces: the zero-symbol subspace and the non-zero-symbol subspace. Thus, measuring the distance between $\text{col}(\mathbf{R}_{\mathbf{h}_k})$ and $\text{col}(\mathbf{R}_{\mathbf{h}_k}^{\text{FF}})$ —which asymptotically must be zero—provides valuable insights into communication performance. Here, $\text{col}(\cdot)$ denotes the subspace spanned by the matrix columns.

There are various methods to measure the distance between subspaces, but the most commonly used in the design of Grassmannian constellations is the *chordal distance*⁴, as it has a direct impact on the error probability [8], [16]. The chordal distance is defined by:

$$d_{\text{ch}}(\mathbf{X}, \mathbf{Y}) = \left(\sum_{i=1}^L \sin^2 \alpha_i \right)^{\frac{1}{2}} = \text{tr}(\mathbf{I} - \mathbf{Y}^H \mathbf{X} \mathbf{X}^H \mathbf{Y})^{\frac{1}{2}}, \quad (15)$$

⁴This is also referred to as *projection F-distance*, *e.g.* [15].

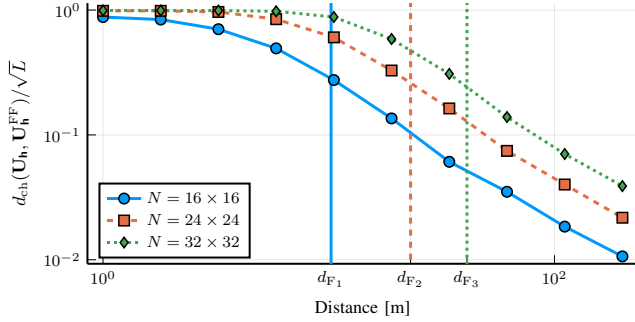


Fig. 3. Chordal distance between $\text{col}(\mathbf{R}_h)$ and $\text{col}(\mathbf{R}_h^{\text{FF}})$ for $N = 16 \times 16$, $N = 24 \times 24$ and $N = 32 \times 32$, in terms of the physical distance between transmitter and receiver. The Fraunhofer distances for each case are indicated as d_{F_1} , d_{F_2} and d_{F_3} .

where \mathbf{X} and \mathbf{Y} are two L -rank matrices and α_i are the principal angles [17], [18] between the subspaces spanned by \mathbf{X} and \mathbf{Y} . Observe that $d_{\text{ch}}(\mathbf{X}, \mathbf{Y}) = 0$ if and only if $\text{col}(\mathbf{X}) = \text{col}(\mathbf{Y})$ and $d_{\text{ch}}(\mathbf{X}, \mathbf{Y}) = \sqrt{L}$ if and only if $\text{col}(\mathbf{X}) \perp \text{col}(\mathbf{Y})$.

Now consider a single UE moving in a straight line from $(1, -30^\circ, -10^\circ)^T$ to $(200, -0.15^\circ, -10^\circ)^T$ under three array configurations: $N = 16 \times 16$, $N = 24 \times 24$ and $N = 32 \times 32$. In Fig. 3, we represent $d_{\text{ch}}(\mathbf{U}_h, \mathbf{U}_h^{\text{FF}})/\sqrt{L}$, where $\mathbf{U}_h, \mathbf{U}_h^{\text{FF}} \in \mathbb{C}^{N \times L}$ are the matrices containing the L eigenvectors associated to the non-zero eigenvalues of \mathbf{R}_h and \mathbf{R}_h^{FF} (the UE subindex has been omitted for simplicity). Differently from the eigenvalues, which were already equal at $r = d_r$, the normalized chordal distance starts being one, that is, the subspaces spanned by \mathbf{R}_h and \mathbf{R}_h^{FF} are orthogonal. Although $d_{\text{ch}}(\mathbf{U}_h, \mathbf{U}_h^{\text{FF}})/\sqrt{L}$ decreases with the distance between transmitter and receiver, at the Fraunhofer distance it still is a 30% of its maximum value, and keeps decreasing at the same rate, suggesting that it is far from converging. In practice, this means that employing the far-field model makes the receiver operate in an appreciably mismatched mode, degrading the performance as it will be shown later.

On the other hand, incrementing the number of antennas (and hence the array aperture) also increases the chordal distance. Indeed, for $N \rightarrow \infty \implies d_{\text{ch}}(\mathbf{U}_h, \mathbf{U}_h^{\text{FF}}) = \sqrt{L}$, and thus $\text{col}(\mathbf{R}_h) \perp \text{col}(\mathbf{R}_h^{\text{FF}})$. This is a specific instance of a well-known result in the large-array literature, namely the asymptotic orthogonality of near-field beamfocusing vectors [19], [20]. To the best of the authors' knowledge, this orthogonality has only been exploited in coherent communication systems. However, it can also be utilized in noncoherent systems to multiplex different UEs.

IV. NUMERICAL RESULTS

In order to verify the impact down to detection of a receiver employing the mismatched model (12) as well as the performance of the suboptimal single-user detector (10), we analyze a system transmitting from a 4-PAM constellation and evaluate its error probability. Specifically, to assess the mismatched mode, we consider a single UE moving away from the BS. On the other hand, the performance of the suboptimal detector is analyzed in a scenario involving five static UEs simultaneously communicating with the same BS.

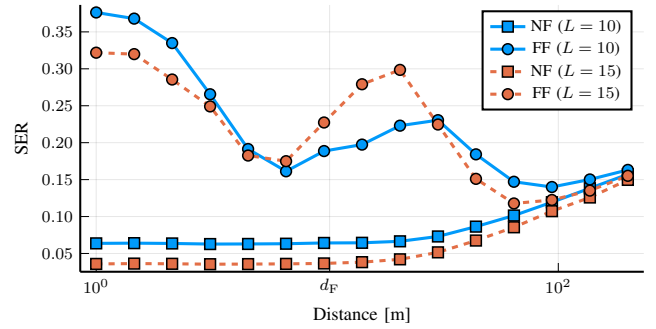


Fig. 4. Error probability of a ML detector employing the exact or mismatched model at different distances. The simulation is performed for $\text{SNR} = 20$ dB.

A. Single-User Mismatched Mode

Let's start with a single UE moving along a straight line from $(1, -30^\circ, -10^\circ)^T$ to $(200, -0.15^\circ, -10^\circ)^T$. The BS implements the receiver from (10), that for $K = 1$ is the ML detector, to decide the transmitted symbol.

To show the impact of operating in a mismatched mode, in Fig. 4 we illustrate the SER of the proposed setup both for a receiver employing the exact correlation model and the mismatched one, for $L = 10$ and $L = 15$. Besides the severe difference between SERs until $10d_F$, using the far-field model may result in unexpected performance behaviors due to the mismatch. Regarding the increase of error probability with distance, even when employing the exact model, it is caused by the loss of resolution between scatterers in the local scattering model. That is, when the distance increases, all signals paths tend to come from the same angle and the rank of the channel correlation matrix goes to one.

The conclusions of this analysis are twofold: first, a receiver should always utilize the exact model, even beyond the Fraunhofer distance; second, noncoherent communication systems can take advantage from near field propagation conditions.

B. Multiuser Detection

Consider a scenario with five UEs. Two of them are located in the near field: $\mathbf{r}_1 = (5, -30^\circ, -20^\circ)^T$ and $\mathbf{r}_2 = (10, -25^\circ, -10^\circ)^T$, whereas the other three are in the far field: $\mathbf{r}_3 = (15, -20^\circ, 0^\circ)^T$, $\mathbf{r}_4 = (20, -15^\circ, 10^\circ)^T$ and $\mathbf{r}_5 = (25, -10^\circ, 20^\circ)^T$. In order to multiplex them, scattering clusters must be separated, so throughout this section we consider $r_s = 1$ m to avoid overlapping. The receiver implements the detector from (10), and its performance with different number of antennas is compared with the scenario where only the UE of interest is present. For the sake of completeness, we also consider the mismatched mode case.

The results of the aforementioned experiment for the fourth UE are shown in Fig. 5 (other UEs are omitted due to the symmetry of the problem). As expected, the SER of the single-user detector tends to that of the optimal detector when the number of antennas increases. In particular, for $N \geq 3500$ both receivers exhibit almost the same performance. On the other hand, the SER of the mismatched receiver is always high, independently of the number of antennas. Finally, we should also remark that the error probability does not vanish with N , as we already pointed out discussing (13) in Sec. II-C.

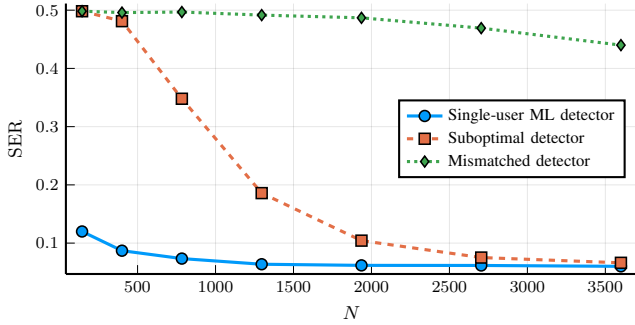


Fig. 5. Error probability of the single-user detector in a multiuser environment for increasing number of antennas. The single-user ML and the mismatched receivers are depicted for comparison and completeness. The SINR is 20 dB.

V. CONCLUSIONS

In this paper we considered the uplink of a noncoherent communication system with arbitrarily located UEs. Focusing on the channel correlation matrices that arise in the exact (*i.e.* near-field) and far-field models, we first showed that although the eigenvalues of both models are almost identical at any distance, the eigenvectors have not converged even at the Fraunhofer distance, suggesting that the near-field model should be employed beyond this boundary. Furthermore, we proved that exploiting large arrays it is possible to multiplex different UEs and achieve near-optimal performance with linear complexity. This suggests that constellations tailored for a single user can also be used in a multiuser environment provided that the number of antennas at the BS is large enough.

REFERENCES

- [1] T. L. Marzetta, *Fundamentals of massive MIMO*. Cambridge, United Kingdom: Cambridge University Press, 2016.
- [2] M. Chafii, L. Bariah, S. Muhaidat, and M. Debbah, “Twelve scientific challenges for 6G: Rethinking the foundations of communications theory,” *IEEE Commun. Surveys Tuts.*, vol. 25, no. 2, pp. 868–904, 2023.
- [3] L. Jing, E. De Carvalho, P. Popovski, and A. Oliveras, “Design and performance analysis of noncoherent detection systems with massive receiver arrays,” *IEEE Trans. Signal Process.*, vol. 64, no. 19, pp. 5000–5010, 2016.
- [4] G. Bacci, L. Sanguinetti, and E. Björnson, “Spherical wavefronts improve MU-MIMO spectral efficiency when using electrically large arrays,” *IEEE Wireless Commun. Lett.*, vol. 12, no. 7, pp. 1219–1223, 2023.
- [5] C. A. Balanis, *Antenna theory: analysis and design*, 4th ed. Hoboken, NJ: Wiley, 2016.
- [6] T. Gong, L. Wei, C. Huang, G. C. Alexandropoulos, M. Debbah, and C. Yuen, “Near-field channel modeling for holographic MIMO communications,” *IEEE Wireless Commun.*, vol. 31, no. 3, pp. 108–116, 2024.
- [7] A. Martí, M. Vilà-Insa, J. Riba, and M. Lamarca, “Constellation design for quadratic detection in noncoherent massive SIMO communications,” in *IEEE 25th Int. Workshop Signal Process. Adv. Wireless Commun. (SPAWC)*, 2024, pp. 566–570.
- [8] D. Cuevas, “Advanced Grassmannian constellation designs for noncoherent MIMO communications,” Ph.D. dissertation, Universidad de Cantabria, 2024.
- [9] Ö. T. Demir, A. Kosasih, and E. Björnson, “Spatial correlation modeling and RS-LS estimation of near-field channels with uniform planar arrays,” in *IEEE 25th Int. Workshop Signal Process. Adv. Wireless Commun. (SPAWC)*, 2024, pp. 236–240.
- [10] Z. Dong and Y. Zeng, “Near-field spatial correlation for extremely large-scale array communications,” *IEEE Commun. Lett.*, vol. 26, no. 7, pp. 1534–1538, 2022.
- [11] J. G. Proakis and M. Salehi, *Digital communications*, 5th ed. Boston, MA: McGraw-Hill, 2008.

- [12] A. Pizzo, L. Sanguinetti, and T. L. Marzetta, “Fourier plane-wave series expansion for holographic MIMO communications,” *IEEE Trans. Wireless Commun.*, vol. 21, no. 9, pp. 6890–6905, 2022.
- [13] M. Vilà-Insa and J. Riba, “Singular detection in noncoherent communications,” 2025, arXiv:2410.15887.
- [14] M. Vilà-Insa, A. Martí, J. Riba, and M. Lamarca, “Quadratic detection in noncoherent massive SIMO systems over correlated channels,” *IEEE Trans. Wireless Commun.*, vol. 23, no. 10, pp. 14 259–14 272, 2024.
- [15] A. Edelman, T. A. Arias, and S. T. Smith, “The geometry of algorithms with orthogonality constraints,” *SIAM Journal on Matrix Analysis and Applications*, vol. 20, no. 2, pp. 303–353, 1998.
- [16] B. Hochwald, T. Marzetta, T. Richardson, W. Sweldens, and R. Urbanke, “Systematic design of unitary space-time constellations,” *IEEE Trans. Inf. Theory*, vol. 46, no. 6, pp. 1962–1973, 2000.
- [17] J. Miao and A. Ben-Israel, “On principal angles between subspaces in \mathbb{R}^n ,” *Linear Algebra and its Applications*, vol. 171, pp. 81–98, 1992.
- [18] A. Galántai and C. J. Hegedűs, “Jordan’s principal angles in complex vector spaces,” *Numerical Linear Algebra with Applications*, vol. 13, no. 7, pp. 589–598, 2006.
- [19] Z. Wu and L. Dai, “Multiple access for near-field communications: SDMA or LDMA?” *IEEE J. Sel. Areas Commun.*, vol. 41, no. 6, pp. 1918–1935, 2023.
- [20] P. Ramezani and E. Björnson, “Near-field beamforming and multiplexing using extremely large aperture arrays,” in *Fundamentals of 6G Communications and Networking*, X. Lin, J. Zhang, Y. Liu, and J. Kim, Eds. Cham, Switzerland: Springer International Publishing, 2024, pp. 317–349.